Journal of Biomedical Optics

BiomedicalOptics.SPIEDigitalLibrary.org

Laser-induced micropore formation and modification of cartilage structure in osteoarthritis healing

Emil Sobol
Olga Baum
Anatoly Shekhter
Sebastian Wachsmann-Hogiu
Alexander Shnirelman
Yulia Alexandrovskaya
Ivan Sadovskyy
Valerii Vinokur

SPIE.

Emil Sobol, Olga Baum, Anatoly Shekhter, Sebastian Wachsmann-Hogiu, Alexander Shnirelman, Yulia Alexandrovskaya, Ivan Sadovskyy, Valerii Vinokur, "Laser-induced micropore formation and modification of cartilage structure in osteoarthritis healing," *J. Biomed. Opt.* **22**(9), 091515 (2017), doi: 10.1117/1.JBO.22.9.091515.

Laser-induced micropore formation and modification of cartilage structure in osteoarthritis healing

Emil Sobol,[a,b,*] Olga Baum,[b] Anatoly Shekhter,[c] Sebastian Wachsmann-Hogiu,[d,e] Alexander Shnirelman,[f] Yulia Alexandrovskaya,[a,b] Ivan Sadovskyy,[g] and Valerii Vinokur[g]
[a]Institute of Applied Physics of the Russian Academy of Sciences, Nizhny Novgorod, Russia
[b]Federal Scientific Research Centre "Crystallography and Photonics" of the Russian Academy of Sciences, Institute of Photonic Technologies, Moscow, Russia
[c]Sechenov First Medical University of Moscow, Institute of Regenerative Medicine, Moscow, Russia
[d]University of California, Center for Biophotonics, Department of Pathology and Laboratory Medicine, Sacramento, California, United States
[e]McGill University, Department of Bioengineering, Montreal, Canada
[f]Concordia University, Department of Mathematics and Statistics, Montreal, Canada
[g]Argonne National Laboratory, Materials Science Division, Argonne, Illinois, United States

Abstract. Pores are vital for functioning of avascular tissues. Laser-induced pores play an important role in the process of cartilage regeneration. The aim of any treatment for osteoarthritis is to repair hyaline-type cartilage. The aims of this study are to answer two questions: (1) How do laser-assisted pores affect the cartilaginous cells to synthesize hyaline cartilage (HC)? and (2) How can the size distribution of pores arising in the course of laser radiation be controlled? We have shown that in cartilage, the pores arise predominately near chondrocytes, which promote nutrition of cells and signal molecular transfer that activates regeneration of cartilage. *In vivo* laser treatment of damaged cartilage of miniature pig joints provides cellular transformation and formation of HC. We propose a simple model of pore formation in biopolymers that paves the way for going beyond the trial-and-error approach when choosing an optimal laser treatment regime. Our findings support the approach toward laser healing of osteoarthritis. [DOI: 10.1117/1.JBO.22.9.091515]

Keywords: lasers; super-resolution microscopy; cartilage regeneration; osteoarthritis; theory of pore formation.

Paper 160807SSR received Nov. 29, 2016; accepted for publication Apr. 28, 2017; published online May 31, 2017.

1 Introduction

Although optical techniques are broadly used in orthopedics and regenerative medicine,[1,2] the long-lasting healing of joint diseases remains a major challenge.[3,4] Even the most advanced treatments of osteoarthritis (OA), based on impeding tissue degeneration, the use of implants that replace the deceased cartilage, or stem cells regenerating the tissue,[4,5] fall short of a permanent cure. Cartilaginous tissue carries supporting functions in the body and must withstand considerable mechanical stress. Hierarchical structure of cartilage on nanoscale, microscale, and macroscale levels is of great importance for its vital function. Cartilage has a very slow turnover of its extracellular matrix (ECM) and low capacity to repair. Cartilage does not contain blood vessels or nerves. Nutrition is supplied to the chondrocytes by diffusion. The compression of the articular cartilage or flexion of the elastic cartilage generates fluid flow, which assists diffusion of nutrients to the chondrocytes.[3]

OA is a degenerative disease of joint cartilage that is the western world's leading cause of pain and disability.[4] Currently, the standard surgical intervention for end-stage degenerative joint pathology is total joint replacement. Early surgical intervention for symptomatic cartilage lesions, including osteotomy and autologous osteochondral graft transplantation, has been suggested to restore normal joint congruity and minimize further joint deterioration.[6] Strategies include cell-based (with or without scaffolds) or whole-tissue transplantation techniques. Although current surgical therapeutic procedures to repair cartilage are clinically useful, they cannot restore a normal articular surface and in many cases result in the growth of inferior quality fibrocartilage.[7] Methods for the full repair of hyaline cartilage (HC) and recovery of its structure and mechanical properties still have not been discovered.[6,8,9]

The methods developed here are based on laser-induced modification of cartilage structure and the recognition of the key role the pores play in the normal functioning of the healthy avascular tissue. The term "pores" for the inhomogeneous tissues is considered as the areas of lesser density and stiffness providing pathways for the liquid mass transfer across the tissue, ensuring its proper nutrition.[10] A porous-elastic model was proposed to describe changes in mechanical properties of HC, fibrous-cartilaginous, and fibrous tissue, and the respective mathematical apparatus was developed.[11,12] The modeling results[11] demonstrated that periodically acting liquid pressure and distending tension regulate synthesis of proteoglycans and collagen fibrillogenesis, filamentous assemblage, and formation of cross-links; they set into order filamentous orientation, causing changes in tissue permeability, modulus of compressibility, and modulus of elasticity.

Traumas and aging can reduce liquid transfer through the tissue, disrupting normal cell nutrition and resulting in the cartilage degeneration.[13]

An effective acceleration of the liquid mass transfer in solids can be achieved by laser irradiation (see Ref. 14 and references therein) as the heterogeneous laser heating induces pores (temporal or permanent) due to inhomogeneous expansion of the material leading to thermomechanical stress.[14] Here, we borrow this approach to adapt it to the biopolymers. We focus on OA healing via pore formation in the cartilage. Recently, we have

*Address all correspondence to: Emil Sobol, E-mail: en.sobol@gmail.com

1083-3668/2017/$25.00 © 2017 SPIE

shown that laser-induced pores play an important role in the process of cartilage regeneration.[15] The role of ECM porosity in tissue nutrition, cell migration, and synthetic activity is investigated concerning the tissue engineering approaches to recover such objects as bones and cartilage.[16,17] However, the size of the pores should be much smaller than the cellular diameter complicating the impregnation of active cells into the already developed porous material.[17]

Recently, we developed a technique for cartilage regeneration in intervertebral discs[18,19] that can be applied for healing of OA via controllable laser-assisted pore formation in cartilage matrix. Pores allow increasing mass transfer in the tissues,[20] in particular, the nutrient liquid transfer to the chondrocytes and the delivery of signal molecules that trigger the processes of cell differentiation and dedifferentiation.[15] The multistage cell transformation process (including cell differentiation and dedifferentiation, proliferation, and synthetic activity) induced by complex effects of heat, mechanical stress, and light adsorption is quite complicated and is not studied in detail. The first aims of this study are to answer two questions: (1) Where should the laser-assisted pores be located to affect the chondrocytes? and (2) how can the size distribution of pores that arise in the course of laser radiation be controlled? Next, we consider the results of the *in vivo* study in miniature pig joint cartilages demonstrating laser-induced cellular transformation and formation of HC. We present evidence that when acting upon the cartilage cells through their immediate environment, in contrast to directly invading them on a molecular level, laser irradiation effectively activates regeneration of HC. Optimization of laser settings allows laser destruction of chondrocytes to be minimized in the course of laser reshaping of cartilage.[21] The laser settings provide lower temperatures for laser regeneration of cartilage than that for laser reshaping; therefore, in this case, thermomechanical effects of laser radiation on chondrocytes should be nondestructive. This establishes the physical and biophysical basis for the healing effect of laser irradiation on damaged and diseased cartilage. To image laser-induced micropores and cellular transformation in cartilage, we employ super-resolution optical, electron, and atomic force microscopy.

2 Materials and Methods

2.1 *Cartilage Ex Vivo Irradiation*

Hip joint articular cartilage was taken from a 6-month-old piglet and was irradiated within 1-h postmortem. We employed an erbium-doped glass fiber laser with the wavelength 1.56 μm (IPG Photonics). The radiation was delivered by applying a fiber with the diameter 600 μm in the contact with the cartilage surface. The spotspacing was 2 to 3 mm. The pulse duration was 100 ms, the pulse repetition rate was 1 Hz. The laser power was 0.9 W, and the exposure time was 10 s (10 pulses). These laser parameters were chosen on the basis of the results of preceding publications.[15,22] The irradiated fragments ($\sim$1 mm^3) and the nonirradiated control samples were extracted using the cylindrical cutting tool, fixed in 10% formalin for histology and in 2.5% glutartaldehyde for transmission electron microscopy (TEM) and processed for the further analysis (48 irradiated fragments and 6 controls).

2.2 *Cartilage In Vivo Irradiation*

Ten 6-month-old miniature pigs were tested in the *in vivo* experiment. The aim of this study was to create minimally traumatic injury of cartilage to allow animals to continue moving. The artificial defects of the size of 2×11 mm were introduced surgically into the hip articular cartilage using a cutter (two defects for each animal on the right and left joint). The depth of the defect was 300 to 400 μm, with care taken not to approach the bone. After 2 months, the defective joints were reopened. The visual observation showed that new, superficial secondary defects (200 to 300-μm deep) occurred in neighboring areas (10 to 15 mm from the primary defect) on the cartilage surface due to abnormal movement of the animals' legs during the preceding 2 months. These secondary defects were examined histologically and considered as a model for degenerated cartilage (OA). The detailed description of such defect modeling is provided in our previous work.[23] In the course of this (secondary) surgery, all defects were irradiated by the laser with the wavelength of 1.56 μm using the parameters described in the cartilage *ex vivo* section. Half of the defects (right or left) were left intact. At 2 and 3 months after irradiation, the joints were opened and the cartilage from the experimental area was extracted for further analysis.

2.3 *Tissue Sampling*

Microscopic investigation using atomic force microscopy (AFM), structural illuminating microscopy (SIM), and TEM methods has been carried out on the tissue sections having 200- to 300-μm depth and 250- to 500-μm radius counted from the symmetry axis of the laser beam.

2.4 *Atomic Force Microscopy*

Cartilage samples for AFM analysis were prepared as described elsewhere.[24] In brief, cartilage fragments were embedded in Tissue-Tek (Tissue-Tek, 4583 Compound, Sakura Finetek Europe, Zoeterwoude, Netherlands) and sectioned on Leica CM3050 S (Nussloch, Germany) cryotome to 20 μm slices and placed onto the glass substrates. Using phosphate-buffered saline (PBS) solution, the samples were washed from the remaining embedding medium and dried at room temperature to constant mass. The images were obtained using the scanning tunnel microscope Nanoscope IIIa (Digital Instruments, Santa Barbara, California). The height profiles were obtained on the air in the tapping mode using the silicon nitride AFM probe (Nanosensors, tip radius <30 nm, scanning rate 1.5 Hz, and resonant frequency 90 to 170 kHz. The collected data were analyzed using Gwyddion 2.03 software (courtesy of David Nečas and Petr Klapetek).

2.5 *Transmission Electron Microscopy*

The cartilage samples were fixed in the 2.5% glutaraldehyde solution in the phosphate buffer and stored at 48°C for 24 h. Then, the samples were immersed into the phosphate buffer two times for 10 to 15 min, dehydrated with the mixture of the absolute alcohol and acetone and embed in the araldite resin. The blocks were cut on ultramicrotome LKB model 3 (Sweden) to obtain the slices of 20- to 30-nm in thickness. The slices were stained with the uranyl acetate, put on the formvar film in the center of a copper grid, and analyzed with the Jeol JEM-1011 transmission electron microscope (Japan) at 80-kV accelerating voltage.

2.6 *Structural Illuminating Microscopy*

The slices of tissues 4- to 5-μm thick were made parallel to the surface (at a distance of 100 to 150 μm from the surface) using

Cryomicrothome Leica CM1900 (Leica Microsystems Nussloch GmbH, Germany) at −15°C with refrigerant Jung tissue freezing medium. The marker Fluo-4 Ca dye (Molecular Probes, Inc.) was applied to manifest Ca^{2+}ions. Images were obtained with the super-resolution microscope, the Optical Microscopy eXperimental (OMX) system v3.0 (Applied Precision, Inc., the GE Healthcare Company). The 60×, 1.45 numerical aperture oil immersion objective was used. The 532-nm laser was used for the fluorescence excitation and the objective immersion oil with the refractive index of 1.514. Super-resolution fluorescence images were reconstructed using softWoRx 2.0 (Applied Precision, Inc.) with the raw data collected with OMX. Reconstructed images were postprocessed and displayed using ImageJ.

2.7 *Histochemistry and Histology*

The samples were fixed in the 10% formalin, stained with the paraffin, and cut on the microtome to obtain the slices of 4- to 5-μm thick. The groups of slices were stained with (a) hematoxylin and eosin, to manifest general structure including cells, (b) picrofuchsin according to van Giesone's protocol for collagen fibrils visualizing, and (c) toluidine blue for acid glycosaminoglycans. The preparations were analyzed using the optical microscope Longway LCX-121S (China). The microphotographs were obtained using the camera model DEM200 MiniSee (China) and processed with the Scope Photo software.

2.8 *Temperature Calculations and Measurements*

Temperature field was calculated on the basis of the solution of thermoconductivity problem for two media (cartilage and quartz optical fiber) described in detail in Ref. 14

$$\frac{\partial T(\mathrm{x},\mathrm{y},\mathrm{z},\tau)}{\partial \tau} = a\left[\frac{\partial^2 T(\mathrm{x},\mathrm{y},\mathrm{z},\tau)}{\partial x^2} + \frac{\partial^2 T(\mathrm{x},\mathrm{y},\mathrm{z},\tau)}{\partial y^2} + \frac{\partial^2 T(\mathrm{x},\mathrm{y},\mathrm{z},\tau)}{\partial z^2}\right] + G(\mathrm{x},\mathrm{y},\mathrm{z},\tau). \quad (1)$$

Here, a is the thermal diffusivity, $G(\mathrm{x},\mathrm{y},\mathrm{z},\tau)$ is the heat source, which is zero for optical fiber

$$G(x,y,z,\tau) = (1-R)q(\tau)\exp\left[-\frac{y^2+z^2}{r_0(x)^2}\right]\exp(-\kappa x), \quad (2)$$

where R is the wavelength-dependent reflectance, κ is the effective absorption coefficient, r_0 is the Gaussian radius, $q(\tau)$ is a periodic step function with pulse duration 100 ms, frequency 1 Hz

$$q_0(\tau) = \left\{\begin{array}{ll} q_0(\tau), & \tau \le 100\ \mathrm{ms} \\ 0, & 100\ \mathrm{ms} < \tau < 1\ s \end{array}\right\}. \quad (3)$$

The boundary conditions for the equality of heat fluxes and temperatures at the surface S between optical fiber and cartilage[25]

$$\lambda_{\mathrm{fiber}}\frac{\partial T_S^{\mathrm{fiber}}(x_{\mathrm{fiber}},y,z,\tau)}{\partial x} = \lambda_{\mathrm{cartilage}}\frac{\partial T_S^{\mathrm{cartilage}}(x_{\mathrm{cartilage}},y,z,\tau)}{\partial x}$$
$$T_S^{\mathrm{fiber}}(x_{\mathrm{fiber}},y,z,\tau) = T_S^{\mathrm{cartilage}}(x_{\mathrm{cartilage}},y,z,\tau), \quad (4)$$

where λ is thermal conductivity.

The heat conductivity problem Eqs. (1) to (4) is solved using the finite difference method in an explicit scheme (temperature on the following time-step can be expressed through the temperatures on the previous time steps). The parameters used for calculations are as follows:[25] $\kappa = 51/\mathrm{cm}$, $r_0 = 250\ \mu\mathrm{m}$, the laser power is 0.9 W, the exposure time is 10 s (pulse duration 100 ms, pulse repetition rate 1 Hz), λ is 0.006 W/cm K, and a is 0.0014 cm^2/s.

Surface temperature of cartilage slab in the course of laser irradiation was measured using IR radiometer (Testo 865, Testo SE & Co. KGaA, Lenzkirch, Germany).

3 Results

3.1 *Ex Vivo Experimental Results*

Laser-induced pores of micron and submicron size in *ex vivo* obtained articular cartilage of the pigs revealed by AFM are shown in Figs. 1(a) and 1(b). The images display the submicron size pores in the tissue matrix with intact periodic collagen fibrils. The green line in Figs. 1(a) and 1(b) corresponds to surface topography presented in graphs [Figs. 1(c) and 1(d)]. The pore size distribution function of the nonirradiated cartilage obtained from the quantitative analysis of its topography shows the maximum at ~40 nm [Fig. 1(e)]. The pore size distribution of the laser-irradiated cartilage demonstrates significantly wider distribution than that for the pristine cartilage, with the maximum at the size of 150 nm [Fig. 1(f)]. These structural peculiarities identified as pores are revealed by SIM [Figs. 1(g), 1(h), and 1(i)]. The nonirradiated cartilage sample, see Fig. 1(g), does not show any pores. For the irradiated cartilage, the size and concentration of the pores depend on the position of the imaged area: the sample taken from the area of the maximal temperature gradient, Fig. 1(i), demonstrates high-porous structure, which is less prominent in the center of the laser beam, Fig. 1(h).

The pores in the laser-irradiated tissue are shown with higher magnification in Fig. 2. The TEM microphotograph of the laser-irradiated cartilage with a pore (the electronically more transparent area) between the chondrocyte (on the right) and the pericellular matrix (PM) (on the left) is shown in Fig. 2(a). The whitish spheroids visualizing a completely transparent area with the diameter from 50 to 150 nm probably can be identified as laser-induced gas bubbles. Figure 2(b) shows two isogenic chondrocytes of the irradiated cartilage surrounded by the pores containing gas bubbles (light spheroids) with diameters from 50 to 180 nm. Figure 2(c) shows such spheroids (gas bubbles) with the diameter from 20 to 200 nm inside the devitalized cell. The nonirradiated control sample contains a minimum of electronically transparent areas and spheroids, see Fig. 2(d).

Although the performed experiments do not allow for the direct monitoring of the dynamics of gas bubble formation, growth, and collapse, we can observe them in the tissue after laser irradiation probably due to their stability.

3.2 *In Vivo Experimental Results*

In the control group, when the animals were not exposed to laser irradiation, the fibrous connective tissue (FT) was revealed histologically in the defect area [Fig. 3(a)]. Sometimes, the fibrous cartilage (FC) was forming under the FT [Fig. 3(a)]. In the laser-irradiated group, the pronounced chondrocyte proliferation in the defect zone was shown in Fig. 3(b). On the defect periphery and in the nearby surroundings outside the defect, numerous

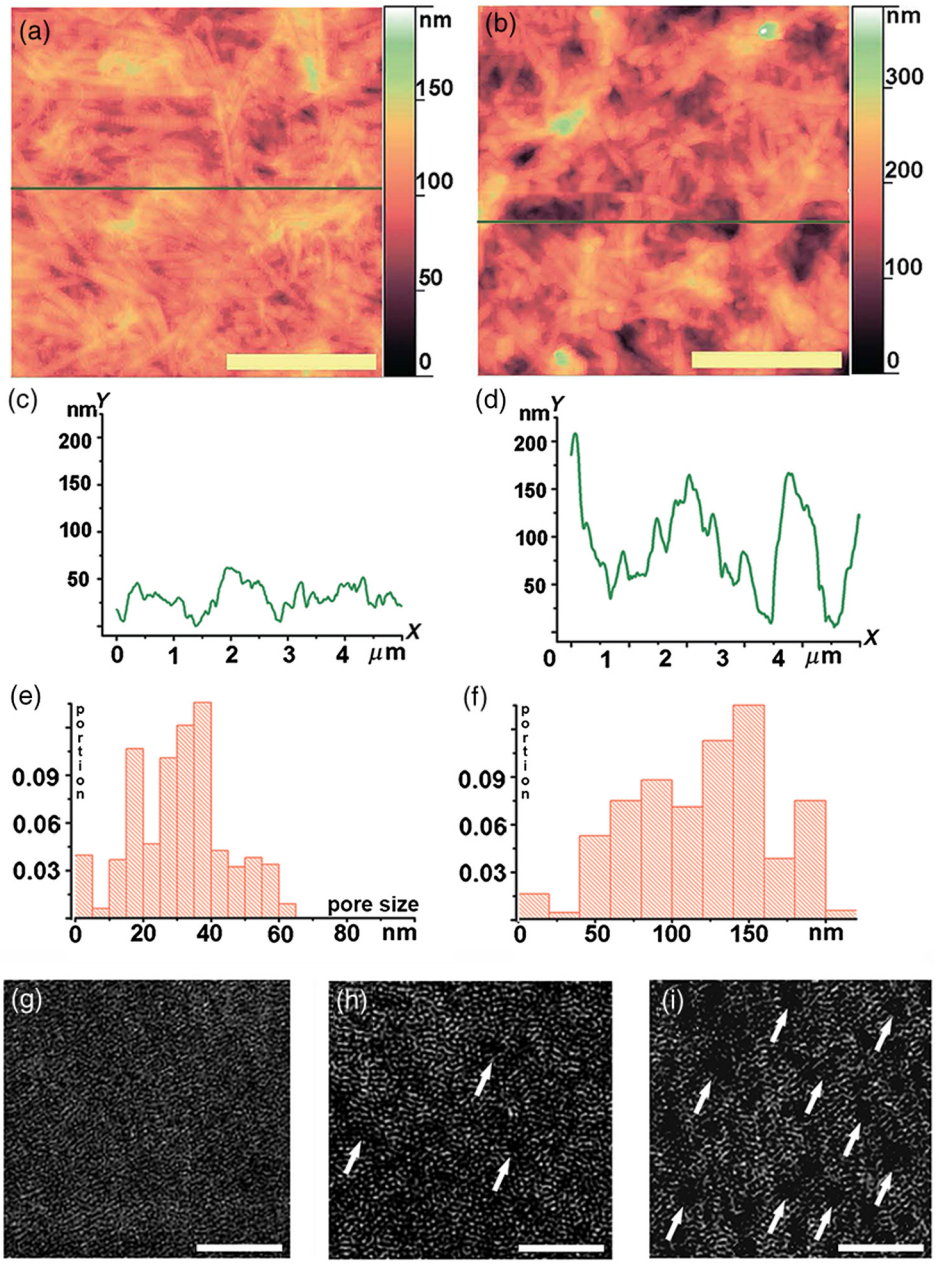

Fig. 1 Laser-induced pores in porcine cartilage. (a) and (b) AFM images of cartilage structure: submicron size pores in cartilage matrix. The bar is 2 μm. (a) Nonirradiated cartilage. The colorimetric scale on the right specifies the correlation between the profile height and the color of the image. The periodic collagen fibrils with the diameter from 50 to 150 nm and the mean period of 62 ± 7 nm are seen. The structure is smooth and the height changes are small. (b) Laser-irradiated cartilage topography. The collagen structure is comparable to that of the pristine one. The presence of dark-colored regions reveals the extended pores (marked with arrows). (c) The texture profile of the nonirradiated cartilage obtained along the green line in nonirradiated cartilage (a). *X*-and *Y*-axes are the coordinate and the texture height value correspondingly. The observed height changes do not exceed tens of nm. (d) The texture profile of the irradiated cartilage. The observed height changes are hundreds of nm that reveals the porous structure. (e) Pore size distribution (arbitrary units) of the nonirradiated cartilage obtained from the quantitative analysis of its topography. The maximum is ~40 nm. (f) Pore size distribution (arbitrary units) of the laser-irradiated cartilage obtained from the quantitative analysis of its topography. The width of the size distribution is substantially wider than that for the intact cartilage. The maximum is ~150 nm. (g) SIM image of the nonirradiated cartilage, the bar is 3 μm. (h) SIM image of the irradiated cartilage in the center of laser spot (temperature maximum), the bar is 3 μm. (i) SIM image of the irradiated cartilage near the maximum of temperature gradient, the bar is 3 μm.

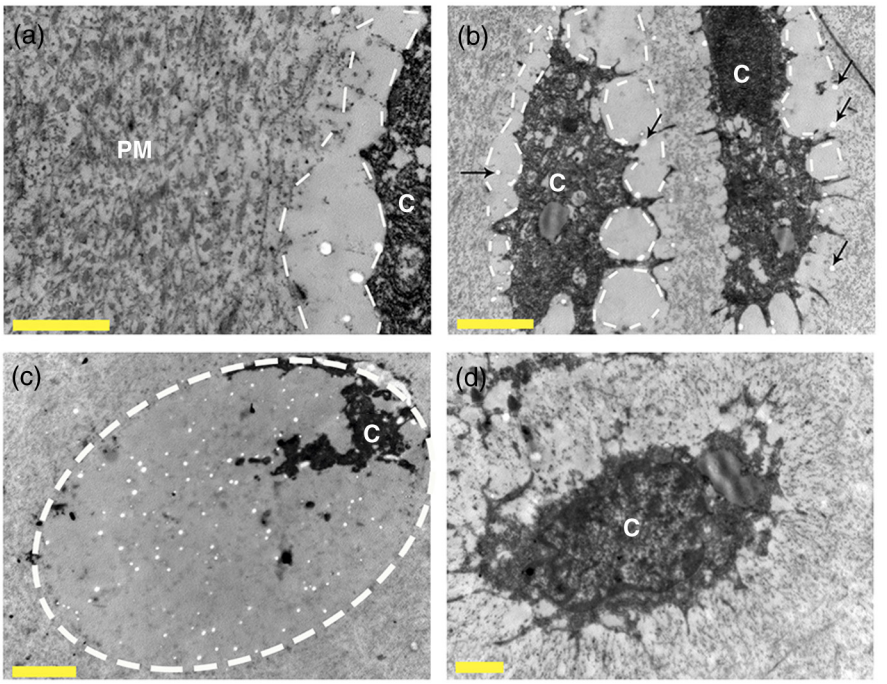

Fig. 2 TEM microphotograph of micropores and gas bubbles in laser-irradiated cartilage. (a) A pore (the electronically transparent area, marked with dashed line) between the chondrocyte (C, on the right) and PM (on the left). The light (white) spheroids with the diameter from 50 to 150 nm probably are the signs of laser-induced gas bubbles, the bar is 1 μm. (b) The two isogenic chondrocytes (C) of the irradiated cartilage surrounded by the pores (marked with the dashed lines) containing light spheroids (gas bubbles) with the diameter from 50 to 180 nm, the bar is 2 μm. (c) Light spheroids (gas bubbles) with the diameter from 20 to 200 nm inside the devitalized cell (marked with dashed line). The disturbed remains of the chondrocytes (C) are on the right, the bar is 2 μm. (d) The representative view of the intact cartilage chondrocyte (C) surrounded by the ECM of small-grained substance, the bar is 1 μm.

large, multicellular clones were forming [Fig. 3(b)]. Figures 3(c)–3(f) shows laser-induced structural alterations that lead to the development of hyaline-type cartilage in miniature pig joints 2 and 3 months after laser treatment. Transformations of the multicellular clones of chondrocytes into the separate, mature chondrocytes that are capable of generating new matrix of the hyaline type are presented in Fig. 3(c). The next sequential steps toward cartilage repair, e.g., the various stages of cartilaginous matrix transformation from the fibrous to fibrous-hyaline and eventually to HC (in 2 months after the laser irradiation), are presented in Figs. 3(d), 3(e). Figure 3(d) shows the FC (bottom right), which transforms into the fibrous-HC (center), and then into the HC (upper left). Figure 3(e) shows fibrous-HC with the typical chondrocytes of HC and matrix looking like the FC. Figure 3(f) shows the final stage of the development of the HC completely filling a cartilage defect of a miniature pig joint 3 months after the laser treatment with the specialized laser settings controlling the formation of the micropores containing transparent spheroids (stable gas bubbles).

3.3 *Theoretical Modeling of the Temperature Effects*

Temperature fields on the surfaces of the cartilage calculated for laser settings used in the experiments are presented in Figs. 4(a) and 4(b). The evolution of the temperature change ΔT at the center of the laser spot following the laser pulse repetition is presented in Fig. 4(a). The spatial distribution of average temperature is shown in Fig. 4(b). The resulting laser heating of the irradiated tissue volume of 1 mm in diameter is nonhomogeneous with the spatial temperature variations of 3°C to 12°C.

3.4 *Thermomechanical Model of the Pore Formation*

Pore formation under laser irradiation is governed by the interplay between the tissue heating and relaxing of its internal and external stresses. To formulate a treatable model for pore formation accounting for both, we consider the tissue as a nonlinear quasi-elastic medium and assume that the thermal destruction of the material can be described as thermally activated breakdown of the chemical bonds.

Here, we select the simplest, two-dimensional version of the problem formulation, which allows us to demonstrate the approach and its main outcomes in the clearest manner. At this stage, it does not take into account important self-healing processes, which may dramatically suppress pore growth. To formulate the model illustrating the pore formation, we will consider cartilage as a nonlinear, practically incompressible elastic medium with a relatively small shear modulus. Cartilage is incompressible because of the practical incompressibility of water, its main constituent. The cartilage stiffness is ensured by its skeleton, comprising macromolecules connected by chemical bonds. Under moderate stress, the probability of the bond breaking is small, and the bond breaking rate is negligible. We quantify the probability of the bond breaking by introducing the corresponding potential barrier so that the probability p of the breaking (per unit time) is defined by the Arrhenius law[26]

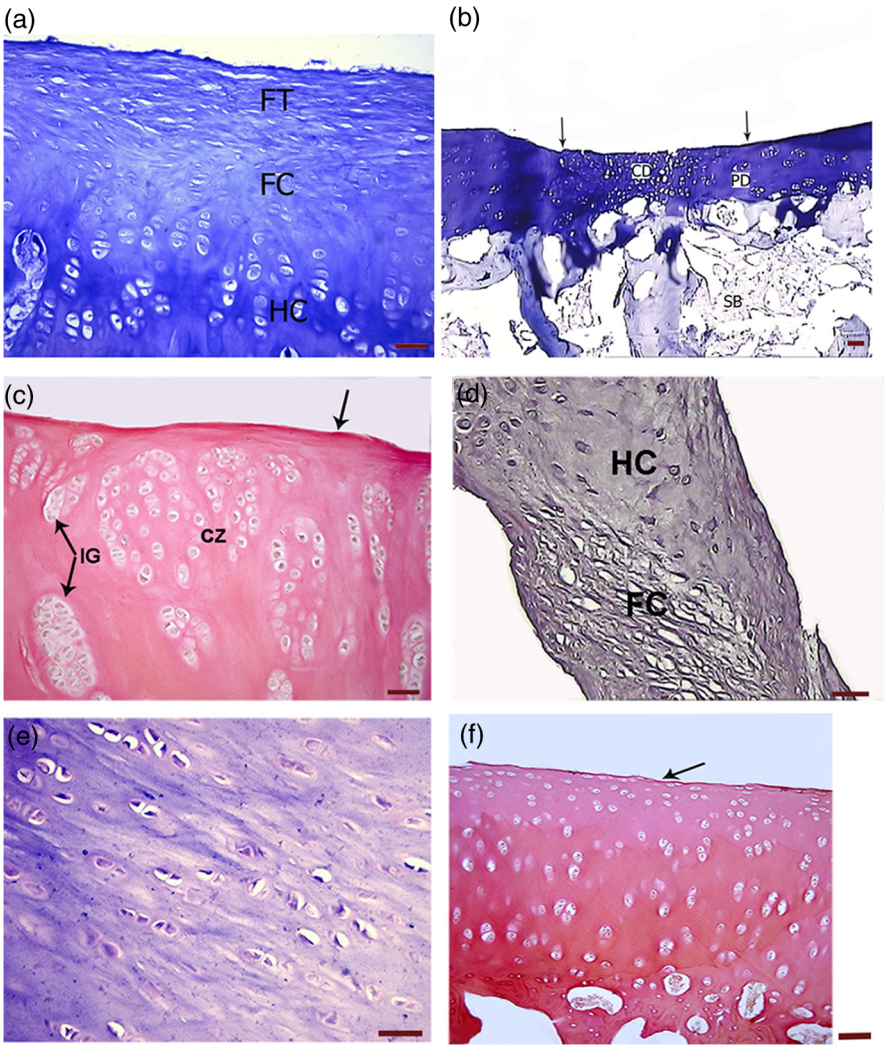

Fig. 3 (a) View of control nonirradiated defect. The defect is filled with FT and FC; residuary HC is under defect; toluidine blue stain, 400×. (b) The common view of the laser-irradiated defect (between the arrows) and surrounding tissues after 2 months. In the center of the defect, there is a noticeable chondrocyte proliferation. On the periphery of the defect, there are large multicellular clones. Under the cartilage plate, there is subchondral bone, toluidine blue stain, 100×. (c)–(e) The images taken 2 months after the laser treatment. (c) Transformation of chondrocytes: isogenous groups IG (multicellular clones) transforms to separate chondrocytes (in the central zone), restoration of lamina splendens (on the top, marked with the arrow), van Gieson stain, 400×, the bar is 50 μm. (d) Growing HC substitutes FC, hematoxylin, and eosin stain, 400×, the bar is 100 μm. (e) Intermediate fibro-HC (in the centum), toluidine blue stain, 400×, the bar is 50 μm. (f) Completely recovered HC and lamina splendens (marked with the arrow) in 3 months after laser treatment of articular cartilage defect, van Gieson stain, 200×, the bar is 100 μm.

$$p = p_0 \exp(-U/RT), \tag{5}$$

where the prefactor p_0 is taken a constant, U is the bond-breaking energy, T is the temperature, and R is the gas constant. Breaking bonds decrease the stiffness of the matrix. We parameterize our cartilage medium by the field $a(x, y)$, which we associate with the bond density, so that $a = 1$ corresponds to the intact cartilage, while $a = 0$ corresponds to the cartilage with the completely destroyed structure, with the zero shear modulus. The inhomogeneity of the cartilage is reflected by the spatial variation of $a(x, y)$.

It is known that the bond-breaking energy would depend not only on what particular chemical bond is involved but also—due to a random environment—upon the bond's spatial position. However, the fact that dynamics of a complex systems governed by the thermally activated behavior is controlled by locally weakest bonds while the neighboring ones are released by avalanche processes, allows to simplify the model taking for U a single typical value.

The natural assumption that the deformation reduces the bond-breaking barrier[27] implies that the pore develops at the spots of the increased mechanical stress. Then, the bond breaking decreases the local stiffness of the matrix, and the system relaxes into a new elastic equilibrium with the new stress distribution.

The deformation of the cartilage and thus the related strain reduces the barrier, $U \to U - \Delta U$, easing the formation of pores.[27] We assume that the difference ΔU is proportional to the elastic energy released as a result of the breaking of one bond

$$\Delta U \sim \delta E/\delta a, \tag{6}$$

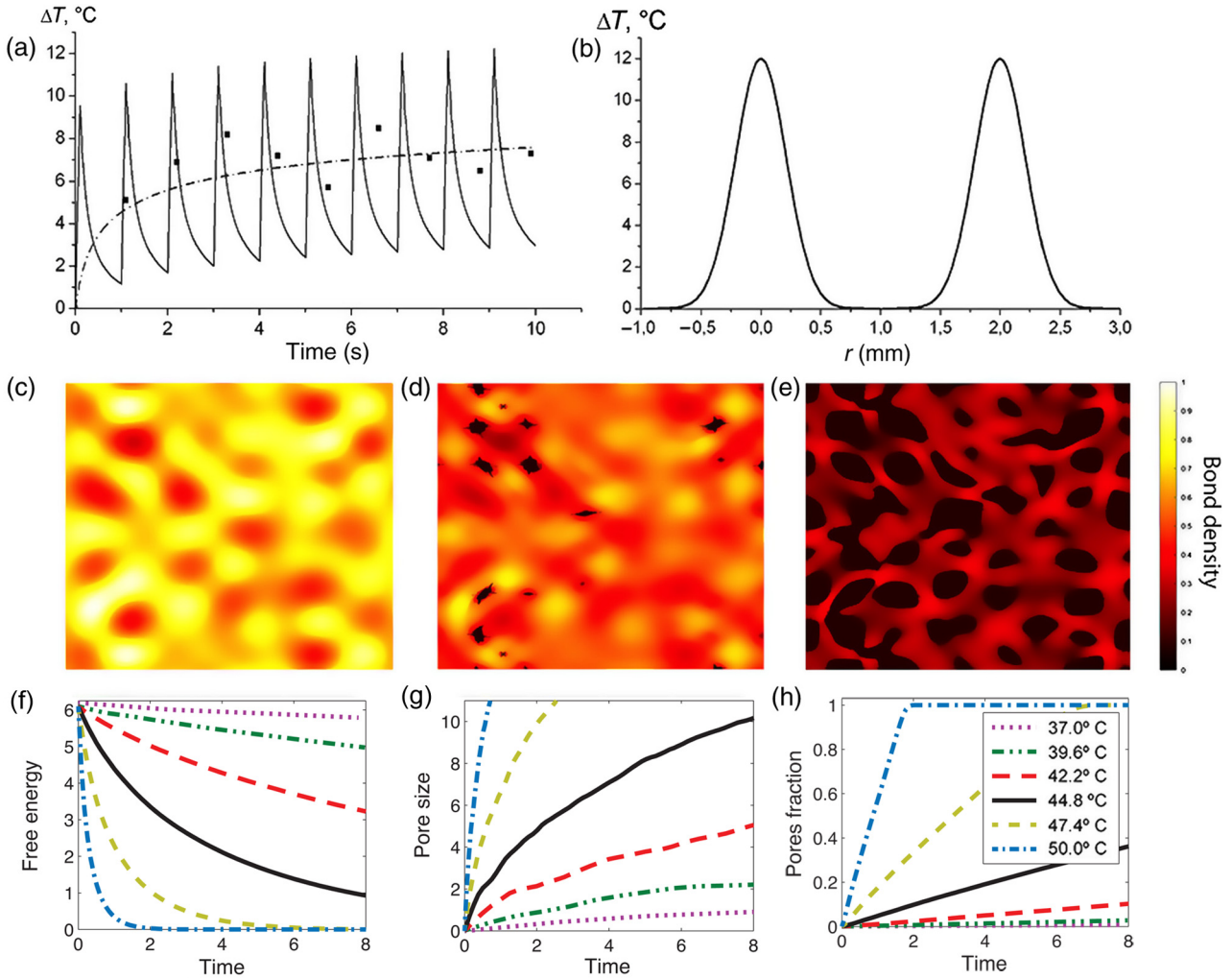

Fig. 4 Numerical simulations of the temperature field and pore formation. (a) Calculated dynamics of the temperature in the center of the laser spot on the surface of the tissue specimen under pulsating irradiation (solid line), average temperature (dashed line), and measured surface temperature (black squares). (b) Spatial distribution of the average temperature in cartilage for the wavelength being 1.56 μm, the Gaussian radius ($1/e$) 250 μm, laser power 0.9 W, time of irradiation 10 s, pulse 100 ms, 1 Hz. (c)–(e) Time evolution of the pores configuration under the permanent heating. (c) Initial distribution of the bond density. (d) Further formation of pores accompanied with the stress relaxation. (e) Final nearly equilibrium pore texture defined by the original cartilage inhomogeneity. (f) Pore-related part of the cartilage free energy at different heating temperatures as function of time. The legend for panels (g)–(h) is given in panel (h). (g) Average pore size as function of time. (h) The relative fraction of the volume occupied by pores as function of time. One sees that under the excessive heating, $T = 50.0$°C, the full burning off of the cartilage occurs during the finite time and the corresponding pore-related free energy relaxes to zero, evidencing the self-consistency of the model.

and the elastic energy of the medium E is defined as

$$E = \int \mathrm{d}x\mathrm{d}y\varepsilon(x, y, a, \partial y/\partial x), \tag{7}$$

where $\varepsilon(x, y, a, \partial y/\partial x)$ is an energy density functional defined by the Mooney–Rivlin model.[28] The linear relaxation equation defining the time evolution of the bond density a

$$\partial a/\partial t = -(a - a_0)p, \tag{8}$$

supplied by the proper boundary conditions and temperature field distribution completes the description of the pores evolution. Here, p is defined by Eqs. (5) and (6), while the right-hand side of Eq. (6), in turn, is defined by the solution of the variation problem with the function $a(x, y, t)$ obtained by this moment, and by the given boundary conditions and temperature field. The physical meaning of the regularizing parameter a_0 is the residual bond density.

The Euler equations and corresponding boundary conditions are not given explicitly since both theoretical study and the numerical solution of the problem are based on the variational formulation.[28] We also do not adopt the usual assumption about the smallness of deformations. The problem reduces to solving the self-consistent system of the elastic equations, including the Arrhenius rate of relaxation and thermal conductivity equations. The obtained closed system of equations and the variation problems defining the behavior of the cartilage under the laser

irradiation are further solved numerically using the finite-elements method.

The experimentally observed laser-induced pores and nanobubbles in the cartilage correspond to moderate laser heating over 10 deg to 12 deg; the temperature time evolution and spatial distribution for the temperature and its gradient are presented in Figs. 4(a) and 4(b). As shown in Fig. 4(a), temperature measurements data confirm the calculation results.

The exemplary initial, nonhomogeneous bond density adopted for calculations is shown in Fig. 4(c). This defines the local elasticity of the cartilage corresponding to the spatially varying stiffnesses of the ECM and chondrons.[16] Applying spatially uniform heating, we arrive at the characteristic pore dynamics shown in Figs. 4(d) and 4(e). In the first stage shown in Fig. 4(d), small pores appear at spots of maximal stress followed by pore growth accompanied by relaxation of the local stresses. At the final stage, we get a pore texture resulting from a relatively long heating of the initially nonuniform matrix, see Fig. 4(e).

To gain an insight into the dynamics of the development of the pore structure, we inspect the temperature evolution of the physical parameters characterizing pores. Figure 4(f) shows the incremental decrease of the pore-related part of the elastic free energy upon the pore formation and the corresponding relaxing stress. Figure 4(g) shows the evolution of the average pore size with the time of heating, and Fig. 4(h) shows the temporal dynamics of the volume fraction occupied by the pores.

4 Discussion

In this study, we show that (1) the pores arise predominately near chondrocytes that promotes nutrition and signaling molecules transfer; (2) *in vivo* laser treatment of miniature pig joint cartilages provides cellular transformation and formation of HC; and (3) outline the ways to control the size and location of laser-induced pores. The described laser effect on the cartilage can be justly attributed to pores and bubbles formation. Crucial for optimizing therapeutic effects is the choice of the laser parameters, including the irradiation wavelength and power, pulse duration and repetition rate, beam spot diameter, and exposure time.[15,20,23] Specifically, the wavelength is taken as 1.56 μm, guaranteeing the penetration depth 0.5 mm, which is defined by the coaction of the light adsorption by the interstitial water and light scattering.[29] The effective length of the beam action results from the interplay of the optical penetration depth and the distance of the heat propagation depending on the time of irradiation t. This distance is estimated as $(at)^{1/2} = 0.4$ mm, where a is cartilage thermal diffusivity 0.0014 cm^2/s. For laser spot diameter of 0.6 mm, the beam heats up $\sim$1 mm^3 of the tissue volume. The calculated temperatures are consistent with the experimental results demonstrate [Fig. 4(a)] that average heating of the irradiated tissue volume of 1-mm in diameter is of 7°C for 10 s. Figure 4(b) shows that the heating is nonhomogeneous with the spatial temperature variations up to 12°C, which is an agreement with temperature measurements performed earlier.[20]

Nonuniform expansion of the tissue, where the expanding hot sections press into the cold surrounding areas, leads to local strains and stress that generate pores, which relax the mechanical stress. Note that the pore formation is one of the known mechanisms of stress relaxation in solids.[30] Pulse repetitive laser radiation induces pulse repetitive heating and repetitive thermomechanical stress affecting cartilaginous cells.[31]

The residual stress in cartilage may alter ECM, in particular, pore structure even after the laser heating stops;[14,29] moreover, in the living systems, the pores can self-heal. Hence, a long-lasting therapeutic effect requires the pores' stability. We have shown that under the chosen laser settings, transparent spheroids (gas bubbles) are induced by the same laser irradiation. Gas bubbles are identified as round formations that are transparent for both electron beams and light. General materials science considerations suggest that bubbles that are point-like inhomogeneities can arrest the collapse of small pores. Note that the gas bubbles that can precipitate due to increasing temperature of the tissue liquid could have disappeared, once the temperature is reduced.[30] It was predicted theoretically that small gas bubbles with the radii of 100 nm can become stable in an electrolyte solution due to absorption of ions on the bubble surface: the Coulomb repulsion of the charges attached to the bubble surface balances the small bubble contraction due to surface tension.[32] The large, nonstable gas bubbles were indeed detected in the spine disc cartilage in the course of laser radiation.[20] But these bubbles were small in the beginning of the process. The evolution of gas bubbles and dynamics of laser-induced structural alterations in the tissue can be detected with light-scattering measurements.[33] The submicron size gas bubbles arise in the regions of the minimal tissue stiffness, predominantly near the cellular boundaries. These laser-induced bubbles can be stabilized by the Ca^{++} and Na^{+} ions presenting in the ECM liquid of the cartilage.

Let us now discuss the *in vivo* study of the cartilaginous cells transformation and formation of the HC. At present, the complex multistep process of the laser-induced cell transformation and tissue regeneration is not studied in detail.[15] The possible mechanisms that can explain the influence of laser-induced pores and bubbles on the singular phases of the multistep process of cartilage regeneration are: (1) the acceleration of liquid and mass transfer within the areas containing laser-induced pores promotes cell nutrition, breath, and transport of signaling molecules;[23] (2) the formation of gas bubbles decreases oxygen concentration in interstitial liquid, and therefore, stimulates cell reparation activity. It is known that synthetic activity of chondrocytes increases with the lowing oxygen concentration;[3] (3) the oscillation of the bubbles under the pulse-periodic laser radiation mechanically affects the chondrocytes stimulating their synthetic activity[23] (the mechanical effect on the cell proliferation and synthesis was studied in Refs. 34–36); and (4) the bubble and pore formation accelerates decomposition of the dead cells, thereby creating free space for the living cells and the growth of the newly synthesized matrix, which is of great importance for cartilage regeneration.[37] An important indicator of the tissue regeneration is the cell turnover rate, i.e., the replacement of the expired cells with the appropriate mature cells. The low turnover rate for chondrocytes is one of the reasons of the limited repair capacity of cartilaginous tissue.[37] Gas bubbles arising inside the devitalized cells with the reduced elasticity, see Fig. 2(c), ease the destruction of such cells, promoting the cell transformation, new tissue growth, and, eventually, regeneration of the cartilage.

Laser-induced formation of the gas bubbles and nanosize pores in the ECM stimulates cascade processes of cellular transformations like differentiation and dedifferentiation of chondrocytes, resulting in the formation of well-organized HC.[15,23] Importantly, pores appear not only within the hottest zones but also in the regions of the minimal Young modulus, i.e., near the

cell surfaces, and in the regions in the neighborhood of the laser spot boundary, where the temperature gradient is maximal. In the absence of inhomogeneities, the heating of the tissue leads to formation of large pores in the area of maximal temperatures, which usually results in the growth of the FC.[23] Morphological images in Fig. 3 show various stages of formation of the HC starting with transformation of cellular structures toward the structural modification of the ECM.

Importantly, in contrast to laser surgeries involving the tissue ablation, the long-term outcome of the laser treatment discussed above rests on stability of the laser-induced structural alterations. Note, in this connection, that overheating above the certain temperature anneals the stabilizing ions from the bubble surface,[38] triggering the collapse of the bubbles and pores in the ECM. The stabilization of laser-assisted gas and pore systems in the tissues can be a reason for long-lasting healing effect in laser reconstruction of spine discs. Thus, to ensure the long-term clinical effect of the laser healing of arthritis[23] and intervertebral disc diseases,[19] strict control over the laser heating regime is required. Since future, *in vivo* studies are required to support the stability of a pore and gas bubble system in cartilage, in contrast to the assertion in Ref. 39, the laser-induced repair of diseased cartilage seems to be possible due to laser-assisted formation of pores and stable gas bubbles.

5 Conclusion

The effect of the laser irradiation is multifold. First, laser irradiation introduces an array of micropores near the cells that enables the flow of liquids and the proper nutrition of the cartilage tissue. Next, it promotes the cell proliferation and the synthetic activity. Thus, laser irradiation promotes the regeneration of HC in the joints.

Disclosures

No conflicts of interest, financial or otherwise, are declared by the authors.

Acknowledgments

The work was supported by the Russian Science Foundation Grant No. 16-15-10274. The *ex vivo* experiments with TEM and SIM are supported by the Russian Foundation for Basic research Grant No. 15-29-04810 and US Civilian Research and Development Foundation Grant No. FSAX-14-60277-0. The work of I.S. and V.V. was supported by the U.S. Department of Energy, Office of Science, Materials Sciences and Engineering Division. The *in vivo* experiments with miniature pigs were approved by the Local Animal Research and Ethics Committee at the Sechenov First Medical University of Moscow. E.S. conceived the concept and designed the experiment; O.B. and S.W-H. performed the experiments with SIM; Y.A. and A.Sh. performed the experiments with TEM; E.S., O.B., and A.Sh. performed the experiments with animals; A.Sn. conceived theoretical concept and developed a theory; V.M.V. analyzed experimental data and developed a theory; I.S. carried out numerical calculations and contributed to theoretical description; all authors contributed to writing this manuscript.

References

1. A. Vitkin et al., "The role of optical techniques in regenerative medicine," in *Optical Techniques in Regenerative Medicine*, S. P. Morgan, F. R. Rose, and S. J. Matcher, Eds., pp. 3–26, CRC Press/Taylor & Francis Group LLC, Boca Raton (2014).
2. S. S. Tomazoni et al., "Isolated and combined effects of photobiomodulation therapy, topical nonsteroidal anti-inflammatory drugs, and physical activity in the treatment of osteoarthritis induced by papain," *J. Biomed. Opt.* **21**(10), 108001 (2016).
3. K. A. Athanasiou, E. M. Darling, and J. C. Hu, *Articular Cartilage Tissue Engineering*, Morgan & Claypool Pub., San Rafael, California (2010).
4. K. A. Athanasiou et al., *Articular Cartilage*, CRC Press, Boca Raton (2013).
5. N. Abdul et al., "Fibrosis is a common outcome following total knee arthroplasty," *Sci. Rep.* **5**, 16469 (2015).
6. E. A. Makris et al., "Repair and tissue engineering techniques for articular cartilage," *Nat. Rev. Rheumatol.* **11**, 21–34 (2015).
7. M. Bonnin et al., *The Knee Joint: Surgical Techniques and Strategies*, Springer, Paris (2012).
8. Y. Peck et al., "A preclinical evaluation of an autologous living hyaline-like cartilaginous graft for articular cartilage repair: a pilot study," *Sci. Rep.* **5**, 16225 (2015).
9. J. C. Hu and K. A. Athanasiou, "A self-assembling process in articular cartilage tissue engineering," *Tissue Eng.* **12**(4), 969–979 (2006).
10. A. R. Jackson and W. Y. Gu, "Transport properties of cartilaginous tissues," *Curr. Rheumatol. Rev.* **5**, 40–50 (2009).
11. E. G. Loboa et al., "Mechanobiology of soft skeletal tissue differentiation—a computational approach of a fiber-reinforced poroelastic model based on homogeneous and isotropic simplifications," *Biomech. Model Mechanobiol.* **2**, 83–96 (2003).
12. P. E. Riches et al., "The internal mechanics of the intervertebral disc under cyclic loading," *J. Biomech.* **35**, 1263–1271 (2002).
13. M. B. Albro et al., "Dynamic loading of immature epiphyseal cartilage pumps nutrients out of vascular canals," *J. Biomech.* **44**, 1654–1659 (2011).
14. E. N. Sobol, *Phase Transformation and Ablation in Laser-Treated Solids*, Wiley and Sons, Inc., New York (1995).
15. E. Sobol et al., "Laser-induced regeneration of cartilage," *J. Biomed. Opt.* **16**, 080902 (2011).
16. M. P. Lutolf and J. A. Hubbell, "Synthetic biomaterials as instructive extracellular microenvironments for morphogenesis in tissue engineering," *Nat. Biotech.* **23**, 47–55 (2005).
17. B. Dhandayuthapani et al., "Polymeric scaffolds in tissue engineering application: a review," *Int. J. Polym. Sci.* **2011**, 1–19 (2011).
18. E. Sobol et al., "Laser reshaping and regeneration of cartilage," *Laser Phys. Lett.* **4**, 488–502 (2007).
19. A. V. Baskov et al., "Long term clinical results in laser reconstruction of spine discs," *J. Spine* **4**, 210 (2015).
20. E. Sobol et al., "Laser regeneration of spine discs cartilage: mechanism, in-vivo study and clinical applications," in *Proceedings of Light-Activated Tissue Regeneration and Therapy Conference*, R. Waynant and D. R. Tata, Eds., pp. 259–266, Springer, Berlin (2008).
21. E. Sobol et al., "Is it possible to perform laser reshaping without dramatic effect on chondrocytes?" *Lasers Surg. Med.* **43**, 911–912 (2011).
22. A. I. Omelchenko and E. N. Sobol, "Optomechanical tests of hydrated biological tissues subjected to laser shaping," *Quantum Electron.* **38**, 269–272 (2008).
23. E. Sobol, A. Shekhter, and A. Baskov, "Lasers in orthopaedic surgery," in *Lasers for Medical Applications: Diagnostics, Therapy and Surgery*, H. Jelinkova, Ed., pp. 628–658, Woodhead Publishing Limited, Oxford (2013).
24. M. Stolz et al., "Early detection of aging cartilage and osteoarthritis in mice and patient samples using atomic force microscopy," *Nat. Nanotechnol.* **4**, 186–192 (2009).
25. O. Baum, "Temperature control system for laser reshaping of nasal septum," *Rus. J. Instrum. Eng.* **58**(10), 847–854 (2015).
26. S. A. Arrhenius, "Über die Dissociationswärme und den Einfluß der Temperatur auf den Dissociationsgrad der Elektrolyte," *Z. Phys. Chem.* **4**, 96–116 (1889).
27. J. Frenkel, *Kinetic Theory of Liquids*, pp. 219–264, Oxford University Press, Oxford (1946).
28. A. I. Shnirelman et al., "A new mechanism for stress relaxation in cartilaginous tissue upon laser heating," *Laser Phys.* **14**, 404–408 (2004).
29. A. V. Yuzhakov et al., "Optical properties of costal cartilage and their variation in the process of non-destructive action of laser radiation with the wavelength 1.56 μm," *Quantum Electron.* **44**, 65–68 (2014).

30. R. W. K. Honeycombe, *The Plastic Deformation of Metals*, Edward Arnold Publishers Ltd., New York (1968).
31. O. I. Baum et al., "Thermomechanical effect of pulse-periodic laser radiation on cartilaginous and eye tissues," *Laser Phys.* **23**, 085602 (2013).
32. P. S. Epstein and M. S. Plesset, "On the stability of gas bubbles in liquid-gas solutions," *J. Chem. Phys.* **18**, 1505–1509 (1950).
33. E. N. Sobol et al., "Time-resolved, light scattering measurements of cartilage and cornea denaturation due to FEL radiation," *J. Biomed. Opt.* **8**(2), 216–222 (2003).
34. C. F. Foldager et al., "Combined 3D and hypoxic culture improves cartilage-specific gene expression in human chondrocytes," *Acta Orthop.* **82**, 234–240 (2011).
35. B. J. F. Wong et al., "Proteoglycan synthesis in porcine nasal cartilage grafts following Nd:YAG ($\lambda = 1.32$ μm) laser-mediated reshaping," *Photochem. Photobiol.* **71**(2), 218–224 (2000).
36. J. Natenstedt et al., "What quantitative mechanical loading stimulates in vitro cultivation best?" *J. Exp. Orthop.* **2**, 15 (2015).
37. A. I. Caplan et al., "Principles of cartilage repair and regeneration," *Clin. Orthop. Rel. Res.* **342**, 254–269 (1997).
38. N. F. Bunkin and F. V. Bunkin, "Bubbstons: stable microscopic gas bubbles is very dilute electrolytic solutions," *Sov. Phys. JETP* **74**, 271–278 (1992).
39. D. J. Huey et al., "Unlike bone, cartilage regeneration remains elusive," *Science* **338**, 917–921 (2012).

Emil Sobol is a biophotonics laboratory head at the Institute of Photon Technologies of the Russian Academy of Sciences (IPT RAS) and senior scientist at the IAP RAS, a member of SPIE and OSA, h-index = 27. His research interests are related to biophotonics, laser–tissues interactions, and laser applications in medicine. He received Theodore Maiman Award from Laser Centers of America in 1994 and Russian National Award "Vocation" for outstanding contribution of nonmedical scientists to medicine in 2001. He has published 190 peer-reviewed scientific papers.

Olga Baum is a senior researcher in the Biophotonics Laboratory at the IPT RAS. Her research interests are related to biophotonics, laser–tissue interactions, and laser applications in medicine. She has published 30 peer-reviewed scientific papers.

Anatoly Shekhter is a head of the Laboratory of Pathomorphology in the Sechenov First Medical University of Moscow. He is a leading specialist in the morphology of connective tissues, regeneration, wound healing, sclerotic, and scar processes. For his research, he was awarded the Governmental Prize of the Russian Federation.

Alexander Shnirelman is a specialist in applied mathematics. He is working on the analytic and numerical study of nonlinear systems (hydrodynamics, MHD, elasticity). He is an author of more than 40 peer-reviewed publications. Currently, he works at Concordia University, Montreal, Canada.

Yulia Alexandrovskaya received her MS degree in physical chemistry from M.V. Lomonosov Moscow State University, Chemical Faculty, in 2011. She is a researcher in the Biophotonics Laboratory at the IPT RAS. Her research interests are laser interactions with biomacromolecules and biological tissues, fabrication of biocompartible nanoparticles, and their application in laser medicine.

Valerii Vinokur is an Argonne Distinguished Fellow. He is a member of the Norwegian National Academy of Science and a fellow of the American Physical Society. He was awarded laureate of the International John Bardeen Prize for outstanding contribution in theory of superconductivity, recipient of the Alexander von Humboldt Award for Senior Scientists (2003, 2013), and laureate of the 2017 International Abrikosov Prize for pioneering concepts describing vortex matter in type II superconductors. He is authored over 350 peer-reviewed publication with over 19,600 citations, h-index = 61.

Biographies for the other authors are not available.